The Effect of an Equatorial Continent on the Tropical Rain Belt. Part I: Annual Mean Changes in the ITCZ

MICHELA BIASUTTI,[a] RICK D. RUSSOTTO,[a] AIKO VOIGT,[b] AND CHARLES C. BLACKMON-LUCA[c]

[a] *Lamont-Doherty Earth Observatory of Columbia University, Palisades, New York*
[b] *Department of Troposphere Research Institute for Meteorology and Climate Research, Karlsruhe Institute of Technology, Karlsruhe, Germany*
[c] *Columbia University, New York, New York*

(Manuscript received 22 September 2020, in final form 17 March 2021)

ABSTRACT: The TRACMIP (Tropical Rain Belts with an Annual Cycle and Continent Model Intercomparison Project) ensemble includes slab-ocean aquaplanet controls and experiments with a highly idealized tropical continent, characterized by modified aquaplanet grid cells with increased evaporative resistance, increased albedo, reduced heat capacity, and no ocean heat transport (zero Q-flux). In the annual mean, an equatorial cold tongue develops west of the continent and induces dry anomalies and a split in the oceanic intertropical convergence zone (ITCZ). Ocean cooling is initiated by advection of cold, dry air from the winter portion of the continent; warm, humid anomalies in the summer portion are restricted to the continent by anomalous surface convergence. The surface energy budget suggests that ocean cooling persists and intensifies because of a positive feedback between a colder surface, drier and colder air, reduced downwelling longwave (LW) flux, and enhanced net surface LW cooling (LW feedback). A feedback between wind, evaporation, and SST (so-called WES feedback) also contributes to the establishment and maintenance of the cold tongue. Simulations with a gray-radiation model and simulations that diverge from protocol (with negligible winter cooling) confirm the importance of moist-radiative feedbacks and of rectification effects on the seasonal cycle. This mechanism coupling the continental and oceanic climate might be relevant to the double ITCZ bias. The key role of the LW feedback suggests that the study of interactions between monsoons and oceanic ITCZs requires full-physics models and a hierarchy of land models that considers evaporative processes alongside heat capacity as a defining characteristic of land.

KEYWORDS: Dynamics; Rainbands; Monsoons; Climate models; Model comparison; Intertropical convergence zone; Bias; Idealized models

1. Introduction

Despite extensive study with a variety of models of increasing complexity and sophistication, some basic theoretical questions about the role of land in shaping Earth's tropical climate and shaping the behavior of the intertropical convergence zone (ITCZ) remain unanswered. In this paper, we examine in detail how the presence of a highly idealized equatorial continent gives rise to an equatorial cold tongue in a motionless ocean and to a latitudinal split in the annual mean ITCZ [Fig. 1; see also Voigt et al. (2016) for a version including more models].

The presence of an upstream continent has long been proposed as necessary to the development of the cold tongue and the northward shift of the ITCZ in the Pacific Ocean basin. The foundational idea in Philander et al. (1996) has been that the presence of South America, a slanted continent that extends from north of the equator to the southern subtropics, allows for the upwelling of cold water along the coast. It is the dynamical response of the ocean that produces the north/south asymmetry in the eastern Pacific, even if feedbacks with cloud changes are also necessary. Other researchers (Takahashi and Battisti 2007; Maroon et al. 2014) have emphasized the role of the Andes mountain range as a barrier to low-level circulation, forcing atmospheric dryness and stronger trade winds in the Southern Hemisphere (SH). In the simulations presented here, though, the representation of the ocean and the characteristics of the continent are both so idealized that none of these mechanisms is active. Yet, the presence of a continent generates a cold tongue, a split of the rainband, and a northward shift of the rain in the northern tropics. How does this happen?

The simulations that we analyze are from the Tropical Rain Belts with an Annual Cycle and Continent Model Intercomparison Project (TRACMIP; Voigt et al. 2016). The ensemble was designed to address the question of the role of land in shaping tropical climate using a multimodel framework that includes full-physics atmospheric general circulation models (GCMs), but at the price of investigating only one land configuration in which a single, geometrically simple continent is stripped down to a few basic physical properties. The control setup (AquaControl) is an aquaplanet with a slab ocean of uniform mixed layer depth and a simple representation of ocean heat transport that mimics the observed zonal mean transport and thus introduces a meridional asymmetry in the climate. The "land" setup [LandControl; modeled after the choice in the classic paper of Chou et al. (2001)] includes a continent that is 45° of longitude wide and extends from 30°S to 30°N. What distinguishes land from ocean is a much-reduced heat capacity, increased albedo, a resistance to surface evaporation, and the lack of meridional heat transport (as specified by "Q-fluxes"). In acknowledgment of the extreme simplification of our parameterization in comparison with true land,

Corresponding author: Michela Biasutti, biasutti@ldeo.columbia.edu

DOI: 10.1175/JCLI-D-20-0739.1

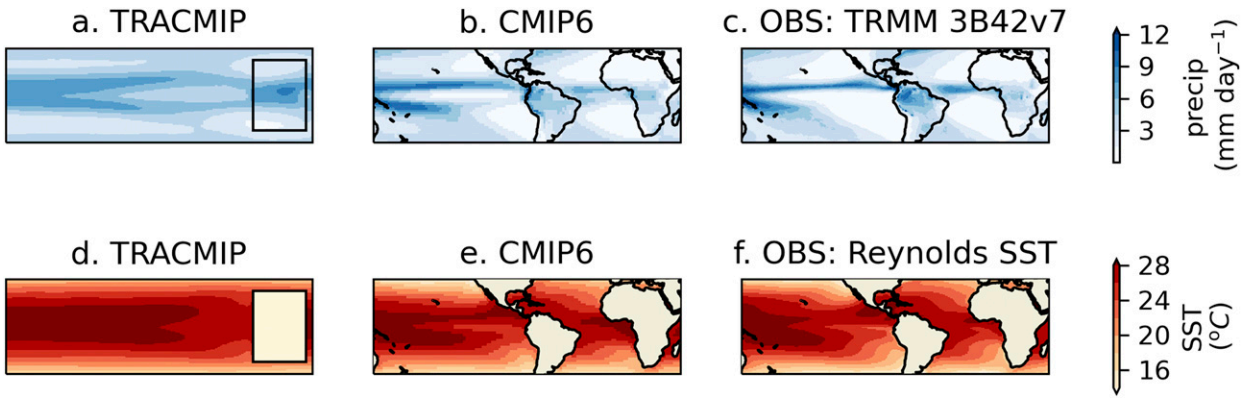

FIG. 1. Annual mean (top) rainfall and (bottom) SST in (a),(d) the ensemble mean of the TRACMIP LandControl simulations; (b),(e) the ensemble mean of the 1979–2014 Historical CMIP6 simulations (Eyring et al. 2016); and (c),(f) observations of precipitation from the TRMM (Huffman et al. 2003) 3B42v7 dataset (1998–2015) and observations of SST from the Reynolds (Reynolds and Smith 1994) dataset (1982–2014).

with a finite soil water content and active vegetation, we have referred to the TRACMIP land as a ''jello'' continent (Voigt et al. 2016). It is only for sake of brevity that we drop the moniker in this paper.

Downstream of the continent, the annual mean rainband, which in the control case has a single broad maximum, is now split into a weaker southern branch and a slightly stronger northern one. The northern ITCZ is located farther north as compared with rainfall farther west in the basin and is only slightly weaker. This configuration is somewhat reminiscent of the Atlantic and, especially, the Pacific Ocean: the eastern basins have a well-defined northern ITCZ and a weaker southern ITCZ (which is present only seasonally in observations, but often is a persistent feature of coupled models; Fig. 1); instead, the western basins are characterized by extensive, uniform rainfall. The asymmetric rainfall configuration is linked to the cooling of the equatorial ocean in a pattern somewhat reminiscent of the Pacific and Atlantic cold tongues (Fig. 1).

Therefore, this paper investigates (i) by what mechanisms does the idealized continent produce these changes in the annual mean rainband in the TRACMIP simulations and (ii) what processes cause intermodel spread in the response. Furthermore, we speculate as to whether such processes are relevant to the real world or realistic model configurations and discuss implications for our understanding of the connection between land monsoons and oceanic ITCZs.

The rest of this paper is organized as follows: In section 2 we describe more details of the model simulations and our analysis procedures. The bulk of our argument is presented in section 3. Focusing on the multimodel mean response, we first show that changes in the rainband can be related to the pattern of SST cooling and, second, describe how the oceanic cooling is established and maintained by latent and longwave fluxes. In section 4 we explore the sources of intermodel scatter. Section 5 summarizes our results and discusses implications for future research and for our broader understanding of the role of continents in climate.

2. Data and methods

a. Data

Voigt et al. (2016) provided the first overview of TRACMIP, describing in detail the protocol of the simulations and the basic features of the response to the imposition of the continent, to the quadrupling of CO_2, and to the change of orbital eccentricity. Here, we consider the TRACMIP control simulations for the aquaplanet and continental setups. AquaControl is an aquaplanet configuration with a slab ocean of 30-m depth, zero eccentricity, atmospheric CO_2 concentrations of 348 ppmv, and a prescribed ocean heat transport convergence similar to that of Earth in the zonal mean [the analytical expression used to prescribe the so-called Q-flux is provided in Voigt et al. (2016)]. The prescribed ocean heat transport breaks the symmetry of the AquaControl climate, creating a warmer Northern Hemisphere (NH) and a slight northern preference for the ITCZ, as expected from theory (Marshall et al. 2014). As we shall see, this meridional asymmetry is amplified by the introduction of the idealized landmass, even though the latter is symmetric about the equator. The jello continent in LandControl is 45° wide in longitude and extending in latitude from 30°N to 30°S; it consists of ocean grid cells with four distinguishing properties: 1) the Q-fluxes representing ocean heat transport convergence are zeroed out in the continent region (note that a uniform compensation over the ocean ensures zero net energy flux anomaly in the global mean), 2) the surface albedo over the continent is increased by 0.07, to mimic the brighter color of land, 3) the heat capacity is reduced by changing the mixed layer depth from 30 to 0.1 m, to mimic a shallow layer of moist soil interacting with the atmosphere, and 4) the evaporation rate coefficient in the bulk moisture flux equation is halved, to mimic the evaporative resistance of a vegetated surface. Soil moisture is not limited, so that surface evaporation is always possible, albeit reduced. No changes in the surface roughness were prescribed.

Table 1 provides a list of TRACMIP models included in this study. All of the TRACMIP models are GCMs with full dynamics and a moist atmosphere and all but one (CaltechGray)

TABLE 1. List of atmospheric GCMs used in this study, along with the coupled Earth system model of which each atmospheric model is a component, if applicable. Only the models that follow protocol (lacking an asterisk) are included in the multimodel means; only the models starting in January are included in the multimodel mean of the transient response. All models except CaltechGray are full-physics GCMs. Citations and additional details such as model resolution are listed in Voigt et al. (2016).

Atmospheric model	Component of	Protocol	January start
CaltechGray	—	Yes	No
CAM3	CCSM3	Yes	Yes
CAM4	CCSM4	Yes	Yes
CAM5Nor	NorESM2	Yes	No
CNRM-AM5	CNRM-CM5	Yes	Yes
ECHAM6.1	MPI-ESM	Yes	Yes
ECHAM6.3*	MPI-ESM	No: Q-flux as in Aquacontrol	Yes
LMDZ5A*	IPSL-CM5A-LR	No: albedo increased by 0.14	Yes
MetUM-CTL*	GA6.0	No: heat capacity as in Aquacontrol	Yes
MetUM-ENT*	GA6.0 (modified)	No: heat capacity as in Aquacontrol	Yes
MIROC5 (atmospheric component)	MIROC5	Yes	Yes
MPAS (atmospheric component)	MPAS	Yes	Yes

include clouds and water vapor–radiation interactions. CaltechGray assumes a fixed emissivity in the atmosphere and contains no clouds (Bordoni and Schneider 2008). Some of the modeling groups participating in the intercomparison did not correctly implement the full land protocol [see the correction published to Voigt et al. (2016)] and we do not consider them in our analysis of the multimodel mean response. Thus, we use an ensemble of eight models for most of our analysis, reduced to seven models (dropping CaltechGray) when radiative fields are concerned.

Yet, we refer to nonprotocol simulations when their having accidentally left out a given land property provides a useful sensitivity test. In particular, we show results from the MetUM models (MetUM-CTL and MetUM-ENT). In these simulations, land points have the correct Q-flux (equal to zero), albedo, and evaporative resistance, but the depth (and hence heat capacity) of the mixed layer are unchanged from those of ocean grid points. Because all those characteristics that *directly* affect the annual mean heat flux into the surface are implemented correctly, we would expect that the annual mean response would also be correct—unless nonlinear effects are important and the seasonal response is rectified. As we shall see, rectification is indeed important, and the MetUM simulations display a muted response. The LMDZ5A model upped the continental albedo twice as much as suggested, and ECHAM6.3 failed to set the implied heat flux to zero over the continent, and these models provide sensitivity tests for those land characteristics. The AM2 land simulations did not include the evaporative resistance and could be used, in principle, as a test of the importance of that land parameter. Unfortunately, AM2 is an outlier in both its AquaControl climate and its LandControl response (Voigt et al. 2016) and we do not feel confident interpreting its behavior as relevant to the role of evaporative resistance in the main ensemble. We therefore exclude AM2 from our analysis.

The CaltechGray model followed protocol [note that the CaltechGray simulations analyzed here are replacements for the ones originally published in Voigt et al. (2016) and were included in the online correction to that paper]. Nevertheless, because it does not include the effect of clouds or water vapor on radiation fluxes, it simulates the effect of evaporation changes only part way, via latent heat fluxes and moist convection. Thus, we can use this model to help us to evaluate *how* evaporative changes affect the final response.

b. Methods

To analyze equilibrium responses to the introduction of the continent into the aquaplanet, we compare the climatologies of LandControl and AquaControl calculated as the average of the last 20 years of simulation. In map plots throughout the paper, we use gray shading to indicate where more than one model disagrees with the consensus on the sign of the anomaly. Areas not shaded are deemed to have robust anomalies.

To quantify the surface radiative effects of atmospheric moisture and clouds and compare them with the radiative flux anomalies expected in a dry atmosphere, we employ radiative kernels for the longwave (LW) component and the approximate partial radiation perturbation (APRP; Taylor et al. 2007) method for the shortwave (SW). We derived climatological zonal mean surface radiative kernels appropriate for an aquaplanet from the full-geometry CESM-CAM5 surface kernels calculated by Pendergrass et al. (2018) by masking out values over and adjacent to the continents, taking a zonal mean across the remaining ocean points, and filling missing values at latitudes with no ocean (i.e., Antarctica) with those from the opposite hemisphere, offset by 6 months to retain the correct seasonality. Kernels derived directly from an aquaplanet GCM (Feldl et al. 2017) were previously used for TRACMIP by Russotto and Biasutti (2020), but these are only available for top-of-atmosphere (TOA) fluxes. To test our method, we have applied the same method described here for the surface kernels to their TOA counterparts and compared our results with the aquaplanet kernels. The agreement is very good within the tropics (less so in the midlatitudes), lending support to our adaptation of the full geometry kernels. The single-layer radiative transfer model of the APRP method is adapted by simple algebraic manipulations to calculate changes in absorbed solar radiation at the surface rather than TOA, similar to Donohoe and Battisti (2011).

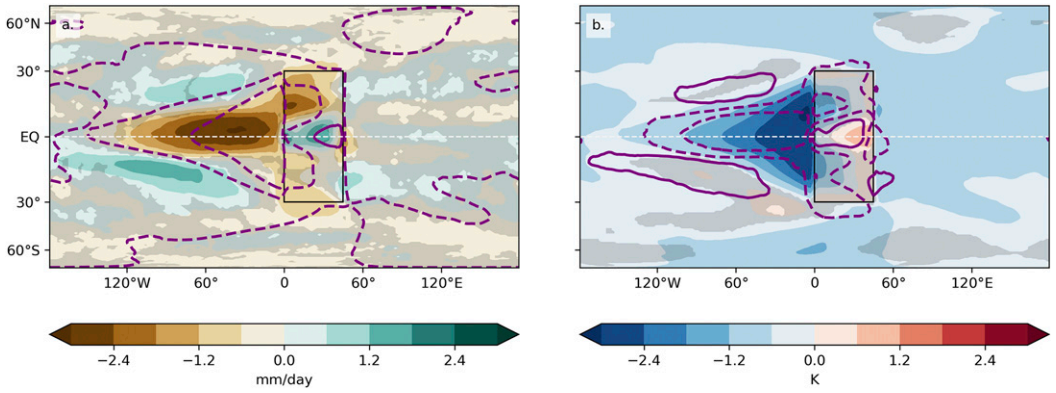

FIG. 2. Ensemble mean of the LandControl − AquaControl annual mean anomalies in precipitation and surface temperature: (a) precipitation (color shading) and SST (contours −1.8, −0.6, and 0.6 K, with negative contours dashed) and (b) SST (color shading) and precipitation (contours −1.8, −0.6, and 0.6 mm day^{-1}, with negative contours dashed). Gray shading indicates where more than one model disagrees with the consensus on the sign of the anomaly.

Gregory regressions (Gregory et al. 2004) on the first 36 months of LandControl − AquaControl anomalies (from which the annual cycle has been subtracted) are used to estimate the rapid adjustments and feedback parameters at each grid point. This procedure assumes that there is a linear response between a given atmospheric variable and the developing surface temperature anomaly directly below. In the traditional application of Gregory regressions, where the variables are global mean temperature and TOA radiative fluxes for global warming simulations, the linearity assumption is typically well satisfied (Gregory and Webb 2008; Andrews et al. 2012), although the slope can change somewhat over time, particularly for coupled models (Armour et al. 2013; Andrews et al. 2015). Since the relevance of point-by-point Gregory regressions to the LandControl − AquaControl anomalies is not a given, we enforce that the linearity assumption holds robustly, as indicated by linear correlation coefficients exceeding 0.5 consistently across the ensemble, and visual inspection of the scatterplots for representative points. These combined requirements limit our analysis of rapid adjustments to LW fluxes and atmospheric humidity.

We interpret the y intercepts of the Gregory regressions (known in the literature as "rapid adjustments" and traditionally corresponding to TOA changes that precede surface temperature changes) as the anomalies that are set in place independently of the *local* surface temperature anomalies. Over the continent, we can think of these anomalies as set by the forcing directly. Away from the continent, we can think of them as an initial remote response to changes elsewhere; because the largest anomalies at the start of the simulation happen over the continent, we specifically interpret the rapid adjustments over the ocean as the initial response to remote changes over the continent. In both cases they represent a response uncomplicated by feedbacks on the local surface temperature. This so-called rapid adjustment response differs from the initial anomalies in that it does not include the seasonal asymmetries that arise in the integration due to the choice of a January initial condition. As we will show later in the paper in Fig. 10, the initial anomalies are opposite north and south of the equator, consistent with a fast response of the continent to solsticial insolation. Instead, the rapid adjustment fields highlight the winter response (which dominates the annual mean response), independent of whether that happens in January (as in the Northern Hemisphere) or later in the seasonal cycle (as in the Southern Hemisphere). The similarity of the rapid adjustments between the protocol models and the MetUM models, in which seasonal anomalies are greatly muted, confirms this interpretation.

3. Robust features of the annual mean response

a. Precipitation

The precipitation response to the equatorial continent (Fig. 2a) is confined to the tropics. Continental anomalies in annual mean rainfall are characterized by dry values in the off-equatorial, or subtropical, regions and by wet values over the equator. The main anomaly induced by the introduction of the continent is to be found not on the continent itself, but over the ocean downstream: a relatively narrow tongue of dry anomalies extends along the equator from the west coast over about 120° of longitude. At their core, the oceanic anomalies are more intense than anomalies over the continent, reaching nearly 3 mm day^{-1} (AquaControl peak precipitation is between 7 and 9 mm day^{-1}). Flanking the dry tongue in the eastern ocean and upstream of the continent at about 20°N/S are weaker positive rainfall anomalies. Overall, the dry anomalies correspond roughly to cold SST anomalies (Fig. 2b), but with some notable differences. Over the continent, the off-equatorial dry anomalies are more extensive and more robust than the corresponding cool anomalies. More strikingly, the anomalies in oceanic rainfall are narrower than the SST cold tongue, although the longitudinal spans of the two fields match. There is a more pronounced meridional asymmetry in rainfall

than in SST: both the dry oceanic anomalies and the wet continental anomalies maximize just north of the equator and the dry anomalies are larger and more robust in the Northern Hemisphere. The meridional asymmetry is a consequence of the small asymmetry in the perturbation and the basic state, due to the prescribed Q-flux.

Figure 3a shows the low-level (925 hPa) mass divergence (shading) and the vertically integrated moisture divergence (contours). Aside from small differences (e.g., the mass divergence over the equatorial ocean is narrower, and the dry anomalies in the northern continent are better defined), the two fields track each other closely, suggesting that, to explain the split in the ITCZ, we need to explain the boundary layer circulation anomalies. Boundary layer pressure gradients are driven from below, by surface temperature gradients (Lindzen and Nigam 1987), but they are also affected by the free troposphere above, especially when convective heating is substantial (Gill 1980), so that the top of the boundary layer is far from being a flat surface. Both mechanisms are at play here. Where the wind convergence is driven primarily from below, the Laplacian of surface temperature (Fig. 3b, shading) shows the same pattern as the mass convergence (Fig. 3a) as expected from Back and Bretherton (2009). This is indeed the case in the tripole of anomalies west of about 60°W, and, to a lesser degree,[1] in the opposite sign tripole over the continent. As we will show more directly in the next section, boundary layer processes are indeed the ultimate cause of the circulation and rainfall anomalies: cold and dry anomalies are advected from the continent to the oceanic region, where they reduce the energy input into the water and lower SST. Thus, it is the boundary layer temperature gradients that drive the large-scale flow. However, feedbacks between rainfall and circulation are large enough that, at the core of the oceanic rainfall anomalies, the Laplacian of SST does not explain the low-level divergence anomalies at equilibrium.

As rainfall anomalies develop downstream of the continent, between 0° and 60°W, the initial low-level mass divergence is modified by the large-scale response to the negative elevated heating (dry precipitation anomalies). In equilibrium, the magnitude of the feedback can be seen in the clear resemblance of the anomalous 200-hPa anomaly field to the canonical Gill pattern (centered on the dry anomalies just downstream of the continent, as seen in Fig. 3b, contour). We note that Chiang et al. (2003) showed that elevated heating is most effective in driving zonal wind anomalies and that, consistently, the divergence out of the cold tongue and dry oceanic anomalies is mostly due to anomalous zonal wind (not shown).

In accordance with quasi-equilibrium theory for convective centers (Emanuel et al. 1994), the peak dry anomalies in the core of the cold tongue correspond to broad low moist static energy (MSE) anomalies (Fig. 3c shows relative (to the global mean values) 925-hPa MSE in shading and specific humidity in contours). Over the continent, MSE anomalies are broader and more robustly negative than the surface temperature

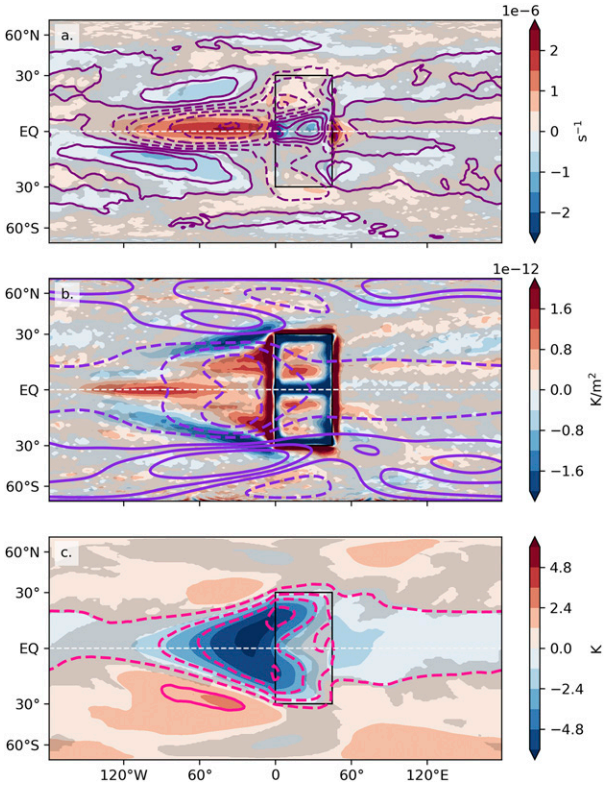

FIG. 3. Ensemble mean of the LandControl − AquaControl annual mean anomalies in (a) 925-hPa mass divergence (shading) and vertically integrated moisture divergence (calculated as $P - E$ so as to include the effect of transients; contours), (b) the Laplacian of SST (shading) and the 200-hPa geopotential height (contour), and (c) the 925-hPa moist static energy (shading; converted to kelvins by dividing by the specific heat capacity of air at constant pressure c_p) and specific humidity (contours). Gray shading indicates where more than one model disagrees with the consensus on the sign of the anomaly.

anomalies and, away from the equator, they reinforce the surface-forced divergence. This suggests that the reduction in evaporation leads to specific and relative humidity reductions that depress convection in the subtropical continental regions, as expected from theory (Emanuel et al. 1994; Lintner and Neelin 2007).

Overall, the rainfall anomalies are closely linked to the surface temperature and humidity anomalies. In particular, the longitudinal extent in the ITCZ split is determined by the shape of the SST cold tongue. Thus, the origin of the SST anomalies is our next focus.

b. SST

It is perhaps surprising that the TRACMIP models simulate weak anomalies where the properties of the slab ocean were changed to mimic land, while they all simulate much stronger anomalies downstream. To make sense of this apparent paradox, in this section we start by looking at the effect of land in terms of the initial energy perturbation at the surface, we compare its components with their counterparts at equilibrium, and

[1] At the coastlines, surface temperature anomalies are weak and are not robust, but they produce prominent edge effects.

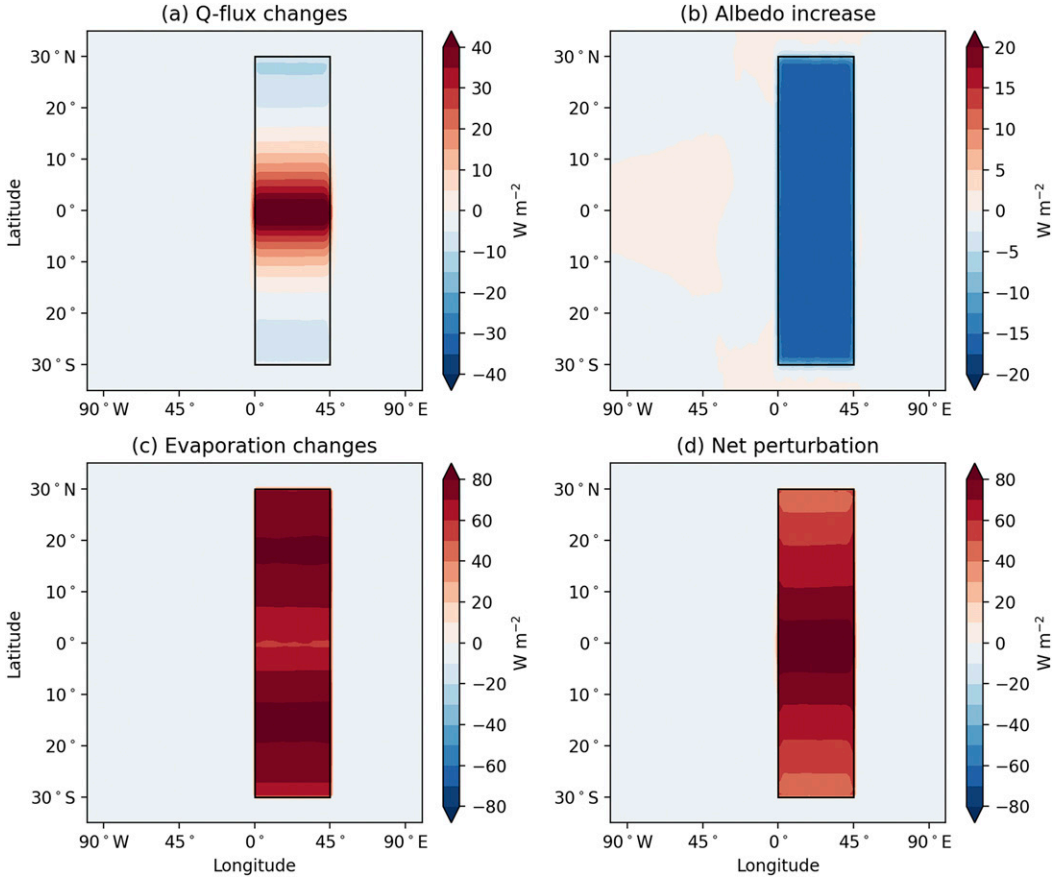

FIG. 4. Multimodel-mean instantaneous changes in surface energy flux associated with various properties of the continent, including (a) the shutoff of ocean heat transport, (b) the increase in albedo, and (c) the reduction of the evaporation coefficient, along with the (d) net perturbation [=(a) + (b) + (c)]. Red colors indicate changes that warm the surface.

we assess the evolution of state variables as the equilibrium is reached.

The most fundamental idealization of land is the shallowing of a slab ocean to reduce its heat capacity. But because this aspect of land is expected to directly affect only the time-varying component of the surface climate and not its time mean (unless rectification effects are large; we will return to this point later), we focus on the other three properties that define land in the TRACMIP ensemble: changes in Q-flux, albedo, and evaporation. Figure 4 shows an offline estimate of the annual-mean energy perturbations that we would expect from these three properties of the continent in the absence of feedbacks, and the sum of these perturbations. Although these are never actually realized in the simulations, we loosely refer to these fields as imposed or initial perturbations because, conceptually, they precede feedbacks. Zeroing out the Q-flux (i.e., LandControl − AquaControl Q-flux; Fig. 4a) has a warming effect at the equator and a cooling effect at the poleward edges of the continent (a small cooling flux over the ocean compensates the continental warming in the global mean). The imposed energy perturbation from the land albedo increase (Fig. 4b) is calculated by multiplying the imposed albedo change by the surface downward SW radiation in AquaControl. The spatially uniform cooling effect over the continent is about 15 W m^{-2}, comparable in magnitude to the other two terms when those are weakest, but much smaller than their peak effect. The initial effect of evaporation reductions (Fig. 4c) is similarly estimated by halving the annual mean surface latent heat flux from AquaControl in the land region; the effect is strong warming everywhere over the continent, but especially in off-equatorial narrow bands around 15°N and 15°S. The combination of these three perturbations (Fig. 4d) forces a warming effect everywhere over the continent, most strongly over the equator where both evaporation reduction and the lack of ocean heat transport combine to warm the surface.

As we have emphasized before, the annual mean equilibrium temperature anomaly looks nothing like what one would expect from looking at the imposed heat flux perturbation: the land warms at the equator and the ocean cools—but the resemblance ends there (Fig. 2). Warming over the continent is confined to just a portion of the equatorial band, while the rest of the continent cools, and the cooling over the ocean is neither uniform nor weak.

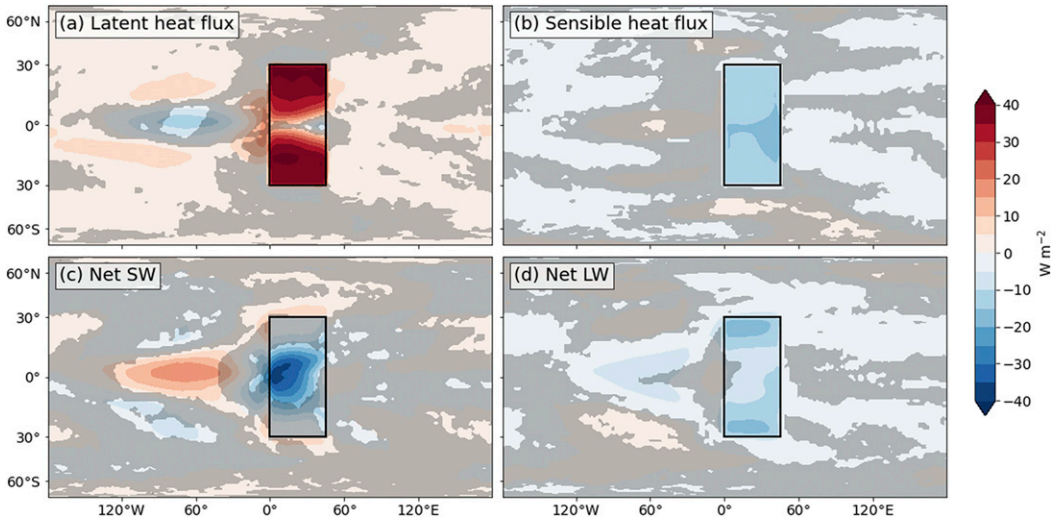

FIG. 5. Multimodel mean anomalies in various terms of the surface energy budget in LandControl minus AquaControl: (a) latent heat flux, (b) sensible heat flux, (c) net SW radiation, and (d) net LW radiation. For all panels, red colors indicate changes that would tend to warm the surface. Gray shading indicates lack of robustness.

The fact that cold anomalies extend from the continental subtropics to the equatorial ocean in the direction of the prevailing trades suggests that the surface circulation ought to be playing a role in establishing these anomalies, but local feedbacks involving clouds and radiation might be just as important in maintaining them. To help us contrast the role of circulation changes to that of local feedbacks, we now examine the structure of the steady-state anomaly response in the surface energy budget terms, which are the end-point response to all changes and feedbacks, and the ''rapid adjustments'' (i.e., those changes whose value is independent of *local* changes in surface temperature) (see section 2b).

Figure 5 shows the equilibrium changes in the components of the surface energy budget (compensating the imposed changes in the Q-flux of Fig. 4): (i) latent heat, (ii) sensible heat, and (iii) and (iv) net SW and LW radiation fluxes. Warm colors indicate warming influences on the surface (maintaining warm anomalies and damping cold anomalies), while cold colors are cooling influences (maintaining cold anomalies and damping warm anomalies). The latent heat flux (Fig. 5a) is generally a warming influence for the continent (although much weaker than in the instantaneous forcing), mostly acting to damp anomalies. It has the opposite effect over the equatorial ocean downstream of the continent, where increases in evaporation help maintain the cold surface temperature anomalies, at least away from the coastline. Closer to the continent and up to 30°W, evaporation changes do not contribute to the annual mean cooling; as we will see, this is a consequence of compensating seasonal shifts. The sensible heat flux (Fig. 5b) opposes, but does not compensate for, the latent heat (anomalies are especially weak over the ocean, as expected). The pattern of net SW flux (Fig. 5c) resembles the pattern of rainfall anomalies, increasing over the equatorial continent and decreasing elsewhere, although changes over the northern and southern continent are not robust. These anomalies mostly act to dampen surface temperature anomalies. In contrast, the net LW flux (Fig. 5d) contributes to maintaining broad cool anomalies over the ocean downstream of the continent, as well as in the northern and southern off-equatorial regions of the continent (the LW flux dampens anomalies over the equatorial band over the continent and just downstream of it). Although annual mean fluxes must add to zero in an equilibrium state, we can interpret these patterns to indicate that the cold tongue is maintained by LW fluxes and, less robustly, latent heat fluxes, and dampened by SW fluxes.

We next further decompose the radiative fluxes. Figure 6 shows the SW flux due to changes in clouds and in water vapor absorption as calculated from the APRP decomposition [results are consistent with the cloud radiative effect (CRE) calculated as the difference of clear-sky and all-sky fluxes]. Most of the SW anomalies are due to changes in clouds, while changes due to humidity represent at most 20% of the signal. In the SW, the effect of clouds is to dampen the surface temperature response everywhere. In the LW, cloud changes play only a minor role: clear-sky anomalies are very similar to all-sky anomalies (not shown). More interesting for the LW signal is the decomposition (obtained from applying the radiative kernels to the equilibrium changes in temperature and humidity; Fig. 7) into components due to changes in surface temperature (the surface Planck response), in atmospheric temperature (the atmospheric Planck effect, pertaining to the vertically uniform component of the temperature change, and the lapse rate effect, pertaining to the vertical structure of the temperature change), and in atmospheric humidity (the optical thickness). Water vapor changes are by far the dominant effect on the continental cooling, but over the cold tongue the humidity and lapse rate have comparable effects, although the greenhouse effect seems to extend farther west. The surface temperature effect is, of course, a damping of anomalies everywhere. We can add the two temperature effects together

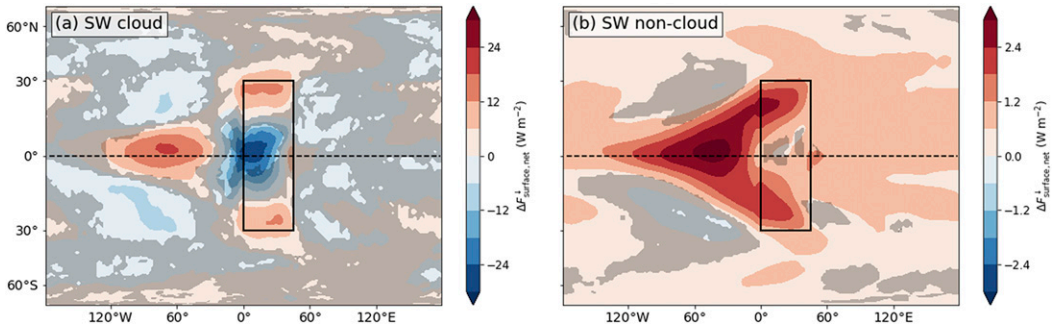

FIG. 6. (a) Cloud and (b) noncloud components of the equilibrium LandControl − AquaControl ensemble mean and annual mean SW flux anomalies at the surface, obtained from approximate partial radiative perturbation analysis. Gray shading indicates lack of robustness. Note that the color scales are different by a factor of 10 in the two plots.

(Fig. 7d) to show that, in the absence of the water vapor anomalies changing the optical thickness of the atmosphere, the LW forcing would become negligible. This is the expectation, then, for the CaltechGray model, which has a gray atmosphere with fixed LW absorption.

We can further investigate how the cold-tongue pattern is established by considering the rapid adjustments of both LW fluxes and humidity (Fig. 8). We recall that the rapid adjustments are derived at each grid point as the *y* intercepts of the Gregory (Gregory et al. 2004) regressions of the transient response of a given field on the value of the local surface temperature and as such they represent changes that are unrelated to *local* changes in surface temperature. When calculated from the LandControl anomalies over the ocean, the rapid adjustments represent the remote responses to the inclusion of the continent that would be simulated if feedbacks associated with local temperature changes were disabled. The extension of the LW cooling (from the subtropical continent onto the ocean) that characterizes the equilibrium anomalies is already clearly established in the rapid adjustment field. This supports the claim that the LW changes are key in the establishment, as well as the maintenance, of the cold tongue. Moreover, the fact that the rapid adjustment signal extends 120° offshore we conclude that the length scale of the oceanic anomalies is set by fast processes (relative to the monthly resolution of the data). We again use radiative kernels to separate the rapid adjustment into the effects of changes in humidity and atmospheric lapse rate (the effect of surface temperature changes on the rapid adjustment is null by definition) and find that water vapor changes are by far the dominant effect on the continental cooling, but that over the cold tongue the humidity and lapse rate have comparable effects. The similarity between the rapid

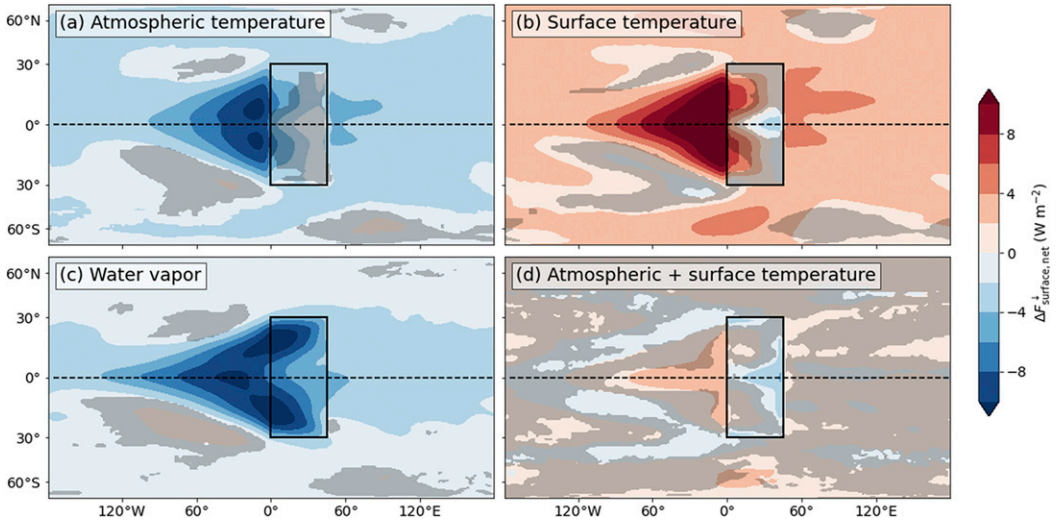

FIG. 7. Components of the equilibrium LandControl − AquaControl ensemble mean and annual mean LW flux anomalies at the surface, obtained from radiative kernels for (a) atmospheric temperature perturbations (i.e., atmospheric Planck effect and lapse rate changes, (b) surface temperature (i.e., Planck emission changes, and (c) water vapor (i.e., optical depth changes). (d) The sum of (a) and (b), representing the downward LW flux resulting from changes in temperature. Gray shading indicates lack of robustness.

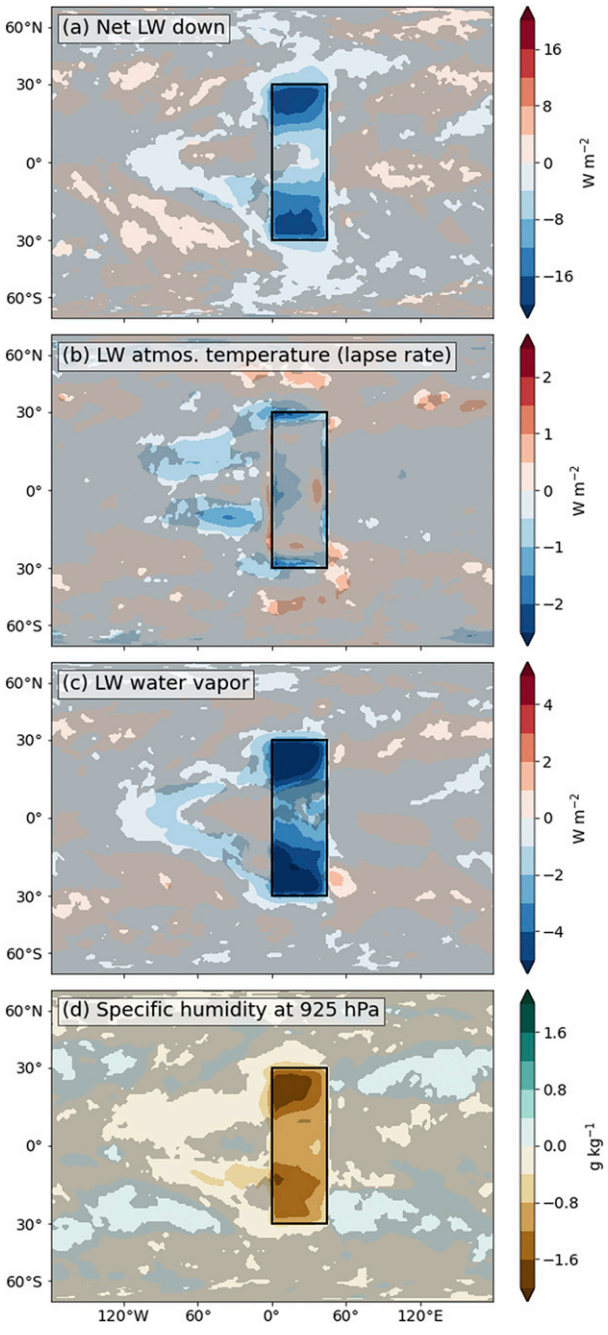

FIG. 8. Rapid adjustments in the net downward LW flux components [(a) total, (b) due to atmospheric temperature changes, and (c) due to water vapor changes] and (d) boundary layer specific humidity. Gray shading indicates where more than one model disagrees with the consensus on the sign of the anomaly.

adjustment and the equilibrium response patterns suggests that changes set in place directly by the presence of the continent are the main drivers of the LW flux anomalies, with temperature-dependent feedbacks and nonlinear behavior playing negligible roles (the direct calculation of the feedback parameter supports this conclusion).

A comparison of the rapid adjustment of boundary layer specific humidity (Fig. 8) with the equilibrium response (Fig. 3c) shows that the effect of advection by the mean trade winds emerges immediately: the easterlies homogenize the humidity anomalies forced by reduced continental evaporation, advecting dry anomalies westward of the continent, as well as moist oceanic air into the eastern half of the continent. This also explains why, at equilibrium, the largest decrease in specific humidity is over the off-equatorial portion of the continent, in correspondence with the greatest direct forcing in evaporation (Fig. 4c), but is concentrated in the western half (Fig. 3c). In contrast, over the core of the cold tongue the initial response is drastically modified by feedbacks: while the initial anomalies are negligible, boundary layer humidity decreases as temperature decreases (so that relative humidity is kept fixed; not shown) and the equilibrium response is the driest at the equator, just off the continent. It is feedbacks, then, that are responsible for the location of the peak equilibrium anomalies at the equator. We investigate this next.

Our interpretation of the origin of temperature anomalies is supported, but also refined, by contrasting the ensemble LandControl − AquaControl response of the full-physics GCMs to the response in the CaltechGray model, as well as those models that, by not having followed protocol, have provided serendipitous sensitivity experiments (Fig. 9). We explore the nonprotocol models first. Both the model that upped the continental albedo twice as much as suggested (LMDZ5A) and the model that failed to set the implied heat flux to zero over the continent (ECHAM6.3) produce anomalies over the ocean very much in line with the ensemble response. This consistency supports our claims that albedo is an overall minor player and that zeroing the heat flux, while important for the continent itself, has minor consequences for the cold tongue. This would leave changes in evaporative resistance as the most likely forcing for the annual mean response. Alternatively, it is possible that changes in heat capacity, which in the absence of nonlinear feedbacks would affect only the time-dependent part of the response, rectify into a time-mean response. This latter effect is tested in the MetUM models (MetUM-CTL and MetUM-ENT), which are full-physics models that implemented all the changes of Fig. 4 correctly but did not reduce the heat capacity of continental grid cells. Because of that, anomalies are muted throughout the year. The response in temperature is qualitatively similar to the ensemble response: warmer anomalies are established over the continent, especially at the equator; cooler anomalies are widespread in the tropical ocean and form a triangular cold tongue downstream of the continent. Nevertheless, there are important differences: the anomalies are of similar weak magnitude over the land and ocean and the cold tongue is confined closer to the coast. This is evident even when anomalies are rescaled to be comparable to the ensemble mean, as shown in Fig. 9, and glaringly obvious when the raw anomalies are considered, as shown below in Figs. 10 and 12. As we will show, the longitudinal extent and the magnitude of the cold-tongue anomalies are related to each other and to the magnitude of the cooling in the subtropical continent.

We also examine the response of the CaltechGray model. The simulations follow protocol, so that all four characteristics

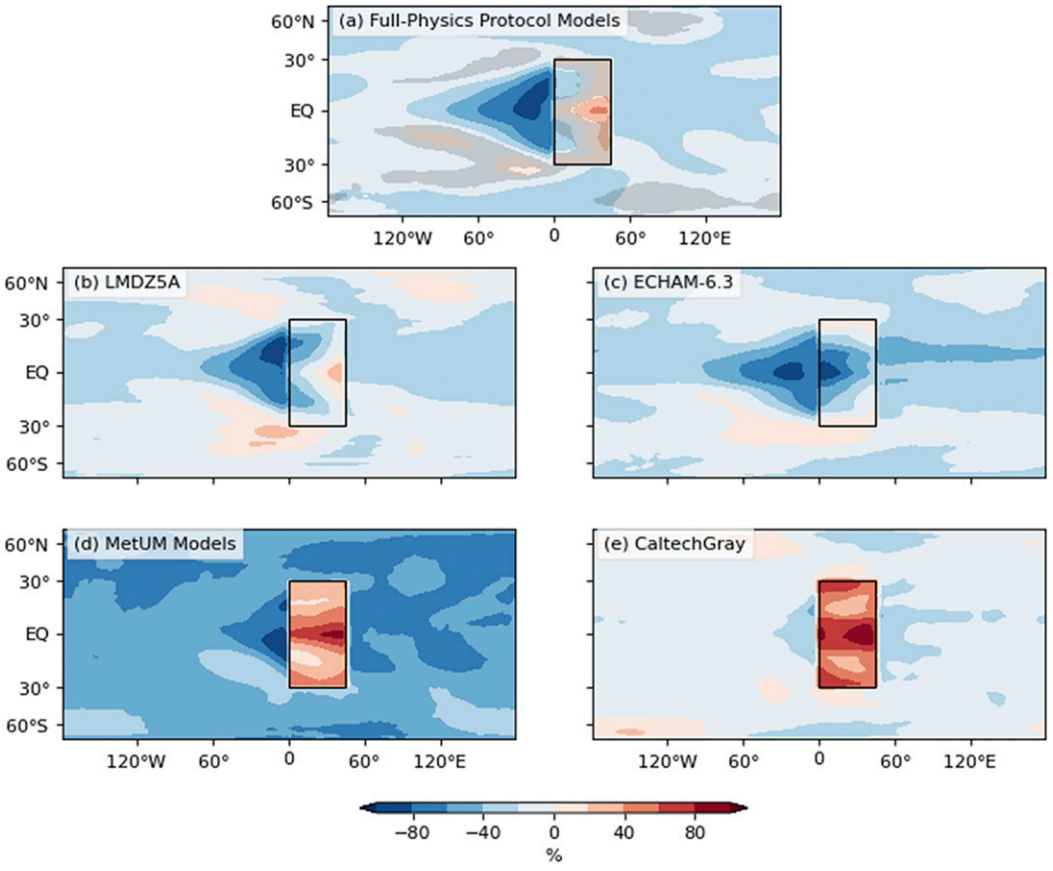

FIG. 9. Annual mean surface temperature LandControl − AquaControl anomalies, expressed as percentage of its global maximum absolute value, in (a) the ensemble average of the full-physics protocol model (gray shading indicates lack of robustness), (b) a model that increased land albedo by 2 times the protocol value, (c) a model that did not zero out the Q-flux representing ocean heat flux convergence over land, (d) the average of the two models that did not reduce the heat capacity of the continent, and (e) the CaltechGray model, which followed protocol but neglects clouds and the radiative effects of water vapor.

of land (no heat transport, enhanced albedo, evaporative resistance, low heat capacity) are considered here. But this idealized model does not include the effect of clouds or water vapor on radiation fluxes, so that the effect of evaporation changes is felt only partway, via its effect on latent heat fluxes and moist convection. Here too, the oceanic anomalies are much reduced, and are in fact a fraction of the continental anomalies. Both in relative (Fig. 9) and absolute terms (Figs. 10 and 12), the cold tongue is scanty and weak. We interpret these results to suggest that a large response in the humidity field is achieved only (i) when a low heat capacity permits large seasonal changes and (ii) when the radiative effects of those large water vapor anomalies set off a feedback between surface temperatures and humidity. Both processes are necessary to the establishment of a prominent cold tongue.

We provide additional support for this view by displaying the evolution of SST anomalies in Fig. 10 (note that despite the large role of seasonality, the annual mean response at the equator is fully established within 6 months). In the full-physics models,[2] within the first month of the simulation large negative anomalies in both temperature and humidity are established in the winter portion of the continent (especially the northwest corner) and are advected just off the coast. Positive humidity anomalies in the summer portion of the continent are the result of competing effects, with the effect of seasonal warming (which would increase humidity) being partly counteracted by the imposed evaporative resistance. SH anomalies are therefore weaker than in the NH, where both the winter cold temperature and the evaporative resistance force a reduction of surface humidity. In addition, the anomalous circulation that converges into the warm continent drastically reduces the easterly winds, blocking humidity, and temperature anomalies from being advected over the ocean. Thus, cold dry anomalies are established over the northern basin, but no warm humid counterpart is established in the southern basin. Two months

[2] Only those models that started their LandControl integrations in January are included in the ensemble mean for this part of the analysis.

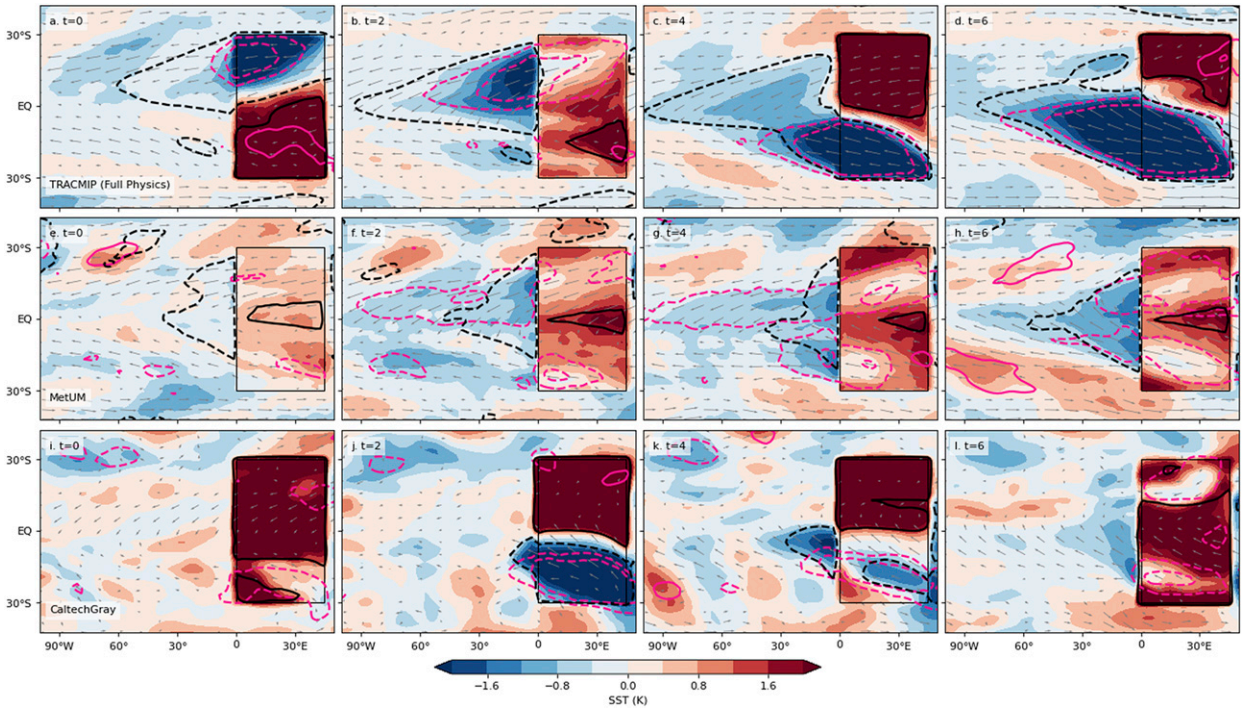

FIG. 10. The evolution of the LandControl − AquaControl anomalies in surface temperature (shading) and 925-hPa specific humidity (pink contours ±1 and ±2 g kg^{-1}, with negative anomalies dashed) and of the LandControl 925-hPa winds (gray arrows; only wind speeds larger than 3 m s^{-1} are plotted) starting with the first month ($t = 0$) of the first year of the LandControl simulations and every other month until the establishment of the annual mean signal in (a)–(d) the ensemble of the full-physics TRACMIP protocol models for which the LandControl starts in January [thus, January ($t = 0$), March ($t = 2$), May ($t = 4$), and July ($t = 6$)], (e)–(h) the average of the MetUM models [January ($t = 0$), March ($t = 2$), May ($t = 4$), and July ($t = 6$)], and (i)–(l) the CaltechGray model [April ($t = 0$), June ($t = 2$), August ($t = 4$) and October ($t = 6$)]. The equilibrium LandControl − AquaControl surface temperature anomalies are also plotted in the thick black lines (±1.2 K).

later (in March) the anomalies over the continent are weakly positive, as one would expect for equinoctial seasons, but cold anomalies have strengthened and expanded over the ocean, reaching nearly as far as their equilibrium response. Correspondingly, the negative humidity anomalies have shifted and are as strong over the ocean as over the NH land. When summer arrives to the NH (May and July), the situation over the continent is reversed and it is the southern portion of the continent that initiates cooling and drying over the ocean. Again, warm continental anomalies are accompanied by much weaker humidity anomalies and these are confined to the western continent by the anomalous circulation. Thus, as the year progresses, the cold tongue over the equator persists, forced alternatively from the north and from the south but intensified and maintained by local feedbacks between humidity and LW fluxes. This pattern is consistent across all the full-physics models.

The same sequence of snapshots for the MetUM models shows similar mechanisms at play, with humidity anomalies developing over the subtropical continent and advected westward. But the lack of winter cooling and drying over the continent mutes the overall signal: both the continent itself and the ocean nearby are warmer than in the TRACMIP-protocol ensemble mean and the SST gradients at the equator are never strong. This, in turn, is reflected in the weak rainfall signal at the equator.

The comparison with the CaltechGray model is made more difficult by the fact that its LandControl simulation starts in April, not January, so that at the beginning of the simulation ($t = 0$; lower left panel in Fig. 10) the springtime continental temperature exerts a small forcing on the nearby ocean. Still, we can see the overall pattern of how the anomalies develop by focusing on the solstice anomalies ($t = 2$, corresponding to June): as in the full-physics models we see strong cold and dry anomalies from the winter (SH) portion of the continent being advected over the adjacent ocean, while the warm anomalies are not matched by wet humidity anomalies and are confined to the NH portion of the continent. The seasonal cooling is, nevertheless, not as strong as in the full-physics ensemble—consistent with the lack of a positive feedback between surface temperature, atmospheric humidity, and longwave energy input. Moreover, over the ocean both the humidity and SST anomalies are narrowly confined and offset from each other, with dry anomalies poleward of SST anomalies throughout the year. Missing an LW water vapor effect, the SST anomalies are neither broadened nor enhanced by radiative effects. Instead, they are a response to the latent heat fluxes that accompany the circulation changes around the

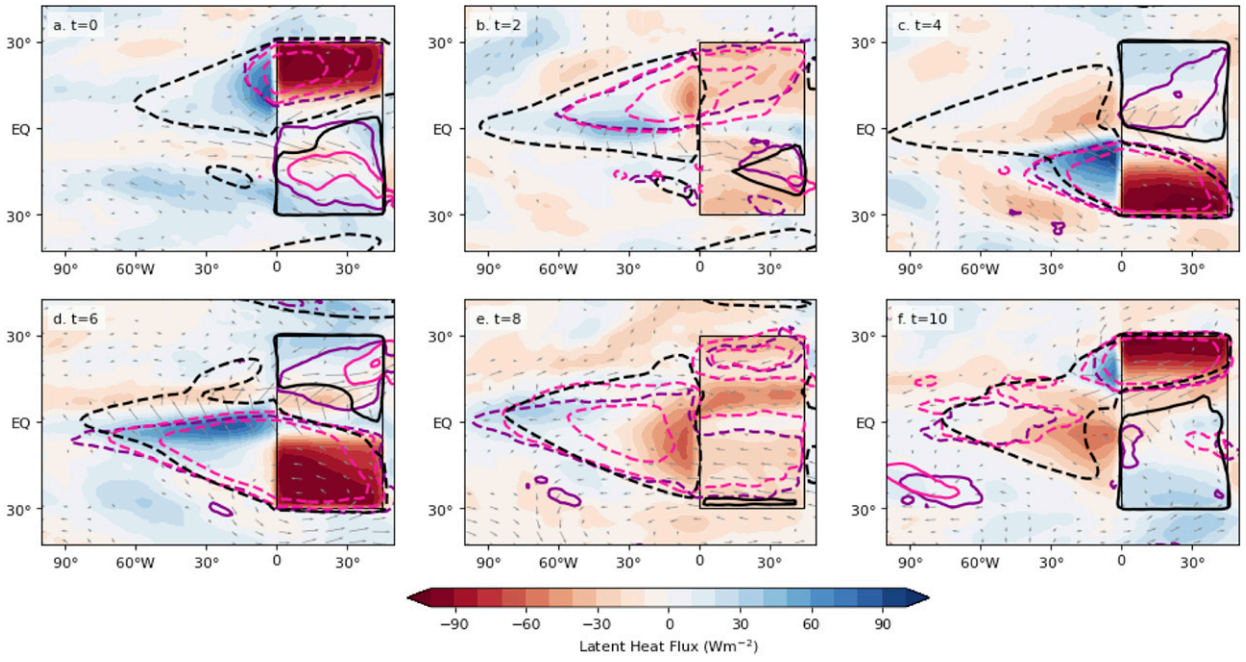

FIG. 11. The evolution of the LandControl − AquaControl anomalies in latent heat flux (shading), 925-hPa winds (gray arrows; only wind speeds larger than 1 m s^{-1} are plotted), LW flux (purple contours ±10 W m^{-2}, with negative anomalies dashed), and 925-hPa specific humidity (pink contours ±1 and ±2 g kg^{-1}, with negative anomalies dashed) for the first year of the LandControl simulations starting with the first month (t = 0) and every other month. The equilibrium LandControl − AquaControl surface temperature anomalies are also plotted in the thick black lines (±1.2 K). All fields are averages across the ensemble of the full-physics TRACMIP protocol models for which the LandControl starts in January.

continent and, as such, they remain confined close to the coastline and they do not develop a clear equatorial peak. Accordingly, there is little change in the ITCZ.

To further investigate the relative role of turbulent and radiative fluxes in establishing the cold tongue in the full-physics models, we show in Fig. 11 the evolution of the latent heat flux anomalies and low-level wind anomalies (shading and vectors), alongside corresponding LW anomalies and low-level humidity (colored contours) for the first year of the simulation (every other month is plotted). As in Fig. 10, the black contour indicates the equilibrium anomalies for the corresponding calendar month. At t = 0 (January), the latent heat anomalies are negative over most of the ocean, consistent with enhanced evaporative cooling in response to the advection of drier continental air, aside from a band of positive latent heat flux just south of the equator, where westerly wind anomalies drive a reduction in evaporation. The large spatial extent of the wind anomalies is responsible for the fact that the footprint of the LH anomalies is much larger than those of LW and humidity. At t = 2, a cross-equatorial wind anomaly extends from the colder NH to the warmer SH and takes the characteristic hook shape of the wind–evaporation–SST (WES) feedback (Xie and Philander 1994) pattern in tropical meridional modes of variability (Chiang and Vimont 2004); the LH cooling is especially strong between 10° and 60°W, where it overlaps with negative anomalies in humidity and LW, but it again extends farther west. At t = 4 (May) the continent has warmed in the SH and the wind anomalies are now blowing from the SH to the NH, warming the equator between 0° and 90°W by reducing evaporative cooling, while enhanced evaporation is confined in the SH, to about 30° off the coast. By t = 6 the WES feedback is established again, and again stronger cooling anomalies correspond to where turbulent and radiative fluxes reinforce each other. At t = 8, the patch where evaporative cooling contributes to the establishment of the cold tongue is very similar to the equilibrium annual mean signal: confined to the equator between 40° and 100°W. At this stage, it is the footprint of the LW anomalies that is consistent with the broad extent of the cold tongue.

In summary, we have shown that wintertime humidity and temperature changes over the continent are advected westward over the ocean; this reduces the LW optical depth of the atmosphere and changes the local lapse rate, leading to surface cooling (the Planck feedback reduces the LW cooling and changes in clouds increase the SW flux, counteracting the positive feedback loop). Seasonal latent heat fluxes are strong and greatly contribute to the cooling of the ocean and drying of the atmosphere above it, but they reverse with the seasons so that they are much weaker in the annual mean, especially close to the continent. Nevertheless, it is the initial circulation anomalies that seem to set the zonal extent of the cold tongue by establishing a domain in which the WES feedback comes to overlap with the LW feedback. In the developing cold tongue, the specific humidity of the boundary layer adjusts to the cold anomalies and the LW fluxes help to maintain cold anomalies so that the end result is cold and dry anomalies that persist at

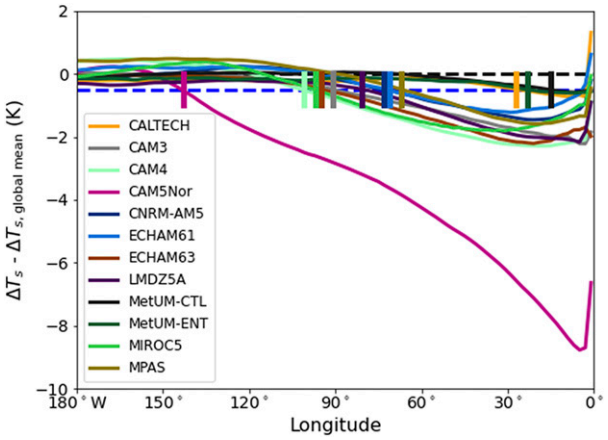

FIG. 12. Profile of equatorial (0.5°N) SST anomalies, relative to global mean temperature changes. The dashed black line is set at zero, the dashed blue line indicates a threshold of −0.5°C, and the vertical segments indicate the longitudes where the anomaly profiles cross said threshold. Models are color coded as indicated in the legend.

the equator year-round. The fact that a cold continent is necessary for the development of the cold tongue was made apparent by the nonprotocol models. Moreover, we can use the scatter across the protocol models to show that there is a robust proportionality between the temperature of the subtropical continent and that of the equatorial cold tongue. This is explored in the next section.

4. Sources of intermodel spread in the strength and extent of the cold tongue

Up to now, we have mostly discussed ensemble mean fields, highlighting the robust aspects of the response in the protocol models. We also explained the weak cold tongue in the CaltechGray simulation by attributing it to the model's neglect of water vapor radiative effects. But what is the reason for the scatter across the full-physics models? In this section, we attempt to account for the differences across the ensemble.

Figure 12 shows the profile of SST anomalies at the equator in the TRACMIP models. Regardless of the scatter across models, the profile of the anomalies is quite similar across the ensemble, so that, in first approximation, models with more extreme peak cold anomalies are the ones with the most extensive cold tongue. We measure the depth of the cold tongue as the minimum negative SST anomalies and the length of the cold tongue as the western longitude when equatorial SST anomalies become weaker than −0.5°C (vertical bars in Fig. 12) and find that the two measures correlate at 0.83 across the eight protocol models. Correlations with bulk measures of the anomalies, such as the area average anomaly in the center (20°–60°W) or the tail (80°–120°W), are also very well correlated between them (correlation coefficient $r = 0.96$) and with depth and length. Thus, we can take the cold-tongue profile to be shape-invariant and describe the strength of the anomalies with a single parameter.

In our discussion of the role of seasonality, we have claimed that strong cooling over the off-equatorial continent is key to the development of the cold tongue. This relationship is also evident in the intermodel scatter, with correlations between annual mean continental cooling and cold-tongue strength around 0.9 (depending on the choice of the cold-tongue index). Thus, the stronger the forcing coming from the continent, the stronger—and farther reaching—is the response downstream.

Moreover, the mechanism that explained the mean response also explains the individual models' responses and the scatter across models. This is shown by the correlations (across the ensemble models) between the equilibrium SST and the surface heat flux anomalies in the cold tongue (Table 2). The LW downward flux (total and net) is the only component of the surface heat flux with significant positive correlation to temperature, indicating that the stronger the cooling effect, the stronger the cold anomalies are. In cases where the correlation is indicative of stronger warming fluxes associated with colder surface temperature, we interpret the relationship to imply causality in the opposite direction: it is the cold temperature that causes a change in clouds and more SW warming, for example. This result is unchanged whether we compute the correlations at the core or at the edge of the cold tongue and whether we use all available models or we exclude the outlier NorESM. We interpret the local correlation with the LW fluxes to indicate that changes in atmospheric humidity and temperature both establish and maintain the response over the equatorial ocean. Using Gregory regressions, we have decomposed the equilibrium LW fluxes and its water vapor and temperature components into rapid adjustments and feedback terms. We find that both the rapid adjustment of the atmospheric temperature (but not the water vapor) and the strength of the water vapor feedback (but not the atmospheric temperature feedback) correlate significantly with the cold anomalies in the ocean—yet we are wary of reading too much in relationships derived by a handful of models when they are not readily physically interpreted. Thus, the relative role of remotely driven rapid adjustments and localized feedbacks in determining the intermodel scatter in LW fluxes is not confidently quantified.

Nevertheless, we maintain that the bulk of the intermodel scatter in the oceanic response is determined from upstream, by the scatter in the land response: recall the 0.9 correlation between cold tongue and continent surface temperature anomalies. What, then, is responsible for the intermodel scatter in the continental response? Table 2 suggests that changes in the SW forcing are the dominant factor (local temperature and SW fluxes correlate above 0.87), while turbulent fluxes and LW fluxes do not have any explanatory power (insignificant correlations, or correlations with the wrong sign). Specifically, cloud changes determine the scatter in SW flux, as indicated by the CRE (the difference in the SW flux for all-sky and clear-sky instances) and confirmed by the APRP calculation, which controls for any confounding effects of pre-existing clouds on the CRE as the surface and atmospheric properties change.

An in-depth examination of one single model is beyond the scope of this paper. Nonetheless, we note that NorESM cools over the equatorial ocean 4 times as much as the rest of the ensemble and over nearly 2 times the longitudinal span. Its cold

TABLE 2. Correlation between surface temperature anomalies and surface fluxes components over the edge of the oceanic cold tongue (80°–120°W, 10°S–10°N), at the core of the cold tongue (20°–60°W, 10°S–10°N), and over the western off-equatorial regions of the continent (0°–25°E and poleward of 12°N/S). In each entry, the first number is calculated for the full-physics models excluding NorESM and the numbers in parentheses are for calculations done including both CaltechGray (with the exception of calculations including LW fluxes and clouds) and NorESM (with the exception LW CRE, for which NorESM data are missing). Boldface numbers indicate correlations that are significant, are robust across the choice of models, and whose sign is indicative of a causality direction in which the scatter across heat fluxes produces the scatter in surface temperature, and not vice versa.

	Ocean (edge)	Ocean (core)	Continent
Latent heat (up)	0.68 (−0.134)	0.05 (−0.04)	0.69 (0.74)
Sensible heat (up)	**−0.94 (−0.78)**	0.09 (−0.18)	0.32 (0.37)
LW down	**0.96 (0.99)**	**0.95 (0.99)**	0.40 (0.17)
LW net down	**0.56 (0.94)**	**0.72 (0.96)**	−0.51 (−0.90)
SW down	0.27 (−0.65)	−0.21 (−0.61)	**0.88 (0.97)**
SW up	−0.05 (−0.27)	−0.18 (−0.22)	0.12 (0.90)
SW net down	0.31 (−0.67)	−0.21 (−0.64)	**0.87 (0.97)**
SW CRE down	0.42 (−0.56)	−0.09 (−0.42)	**0.91 (0.98)**
LW CRE down	0.037	**0.64**	−0.94
SW net down (APRP)	0.45 (−0.59)	−0.122 (−0.56)	**0.92 (0.97)**

tongue is also stronger than we would expect from the strength of its continental cooling. We have noticed that this is the only model in which the cloud radiative forcing depends nonmonotonically on the surface temperature, suggesting that the model is switching from deep to low clouds at cold enough temperatures (and thus going from a weak CRE regime to a strong CRE regime). We speculate that this switch might contribute to its outlier behavior, but targeted sensitivity experiments would be necessary to substantiate this hunch.

In summary, the strength and extent of the cold tongue vary in tandem and are, in large part, determined by how cold the continent gets; that in turn is a function of the how each model simulates SW cloud processes.

5. Discussion and conclusions

The TRACMIP simulations indicate that the presence of a continent induces a cold tongue in the equatorial ocean downstream via purely thermodynamic ocean–atmosphere coupling: cold and dry air is advected by the trade winds from the winter portion of the continent over the ocean, which is cooled and dried in response via surface fluxes. The seasonal SST changes are forced in large part by latent heat fluxes, but they persist and develop into large year-round anomalies centered at the equator through a positive feedback between cold SST, low atmospheric humidity and temperature, and decreased greenhouse warming.

A thermodynamic coupling between the atmosphere and the equatorial cold tongue has been discussed in the literature before, but the focus has been on the role of clouds and wind-induced turbulent heat fluxes. Philander et al. (1996) suggested that a thermodynamic feedback between cold ocean temperatures and stratus decks is instrumental in maintaining the climatological cold tongue in place and the ITCZ north of the equator in the Pacific. In the TRACMIP experiments, the lack of upwelling causes our basic state to be too warm to allow extensive stratus decks, and the role of clouds is muted over the ocean, with the possible exception of the NorESM model. Xie and Philander (1994) introduced the idea of a feedback between the speed of the surface wind, evaporation, and the maintenance of meridional gradients across the equator [the wind–evaporation–SST (WES) feedback]. We expect this mechanism to be at play in the creation of the seasonal anomalies, when cross-equatorial gradients are large; yet, in the annual mean, the latent fluxes are acting to dampen the equatorial anomalies and smooth out the gradients. If the CaltechGray model is representative of more complex models, at least as it pertains to this feedback, it would indicate that the WES mechanism is not, by itself, sufficient to create an annual mean cold tongue that extends past 20° offshore.

The cold-tongue SST anomalies that develop in the lee of the TRACMIP continent are substantial: typically they range between −1° and −2°C at their peak and they do not weaken past −0.5°C until 65°–100° of longitude past the coastline. This suggests that the downstream effect of land ought to be considered when studying the cold-tongue climatology and variability and their biased representations in more realistic models. Below, we list possible phenomena in which the continent–ocean coupling at play in TRACMIP might be of relevance to different phenomena and suggest further avenues of research.

In explaining multidecadal variability, Clement et al. (2011) and Bellomo et al. (2014) highlighted the role of thermodynamic coupling between the ocean and atmosphere in driving ENSO-like anomalies in the Pacific, suggesting a role both for latent heat fluxes and for cloud radiative effects. In our setup, turbulent fluxes and cloud processes are active, but the main sources of anomalies are cold and dry anomalies that generate over the continent at the seasonal time scale. For the mechanisms described in this paper to be relevant to climate variability, persistent cold or dry continental anomalies would have to be established. We can imagine two pathways: either via the action of direct external forcing (e.g., from land use or aerosols) or forced by ocean variability, onto which land would feed back as described above. Whether these anomalies would be large enough to matter,

relative to anomalies forced by ocean dynamics and stratus deck feedbacks, is an open question left for future study.

The processes responsible for the evolution of the TRACMIP LandControl − AquaControl anomalies depend on the basic features of a cold and dry winter continent, so we can assume that the processes themselves are also at play in the real world as long as we allow for their effects to be modified in light of different continental characteristics. For example, we can speculate that the narrow Central American landmass would not be as effective as South America in forcing oceanic cooling, making the southeastern Pacific colder than the northeastern Pacific. The presence of the Andes would also be expected to amplify both the drying and the cooling in the SH (Takahashi and Battisti 2007). In contrast, we would expect that the dryness of the Sahara Desert would amplify the cooling of the Atlantic Ocean in the northern tropics. In both basins, the final state of the tropical oceans will depend, of course, on the interactions of these effects with ocean upwelling and, more generally, ocean dynamics. Still, we maintain that the processes at play in TRACMIP must also be at play in simulations with realistic continental configurations, and we suggest that they might help explain GCM biases in the double ITCZ region. In particular, our findings are consistent with those of Zhou and Xie (2017), who showed that the CMIP5 spread in the double-ITCZ bias in coupled configurations can be traced back to biases in land surface temperature in uncoupled configurations. Unsurprisingly, clouds are the main culprit for the spread of surface temperatures in the highly idealized TRACMIP continent but, over realistic land, surface temperature biases may be ascribed to either surface albedo or other mechanisms involving clouds, aerosol, or land processes.

We speculate that the thermodynamic driving of equatorial cold anomalies in the eastern Pacific and Atlantic could change in a warmer world. On one hand, we expect the contrast in specific humidity between the continent and the nearby ocean to intensify, and this effect would drive a colder cold tongue. On the other hand, the circulation is expected to weaken and the importance of anomalous LW warming to be reduced relative to the enhanced background state, so that a weakening of this mechanism could also be expected. Given the importance of the pattern of SST changes in driving regional anomalies (e.g., Chadwick et al. 2014), and given the open questions surrounding the El Niño– or La Niña–like warming (Seager et al. 2019), the question of continental influence on the cold-tongue response to anthropogenic forcing is worth further research but remains beyond the scope of this paper.

In this study we have hinted at the fact that seasonal variations over land depend most strongly on the change in heat capacity, as both gradients in atmospheric humidity and the pattern of convergence into the summer continent and divergence out of the winter continent depend on the seasonal differential heating north and south of the equator. Thus, one should be justified in considering only this characteristic of land when designing idealized experiments focused on the climatological monsoon circulation. This assumption was verified, at least partially, in the seminal work of Chou et al. (2001) and is at the basis of much theoretical literature on fundamental monsoon dynamics (e.g., Bordoni and Schneider 2008; Maroon and Frierson 2016; Zhou and Xie 2018). Nevertheless, if one is interested in the connection between regional precipitation centers—and, in particular, in the coherence between regional monsoons and the oceanic or zonal mean ITCZ in responding to external forcings (Biasutti et al. 2018; Atwood et al. 2020)—then the magnitude of the evaporation anomalies over land matters greatly. This class of problems, we maintain, requires an expanded hierarchy of land models, one that considers evapotranspiration processes alongside heat capacity as a defining characteristic of land.

Acknowledgments. Michela Biasutti, Rick Russotto, Aiko Voigt, and the overall TRACMIP project are supported by the National Science Foundation under Award AGS-1565522. Charles Blackmon-Luca's participation in this project was supported by the Columbia University Earth Institute. Voigt received support from the German Ministry of Education and Research (BMBF) and FONA: Research for Sustainable Development (https://www.fona.de/en/) under Grant 01LK1509. Biasutti was supported by U.S. Department of Energy BER Award DE-SC0014423. We thank the modeling groups responsible for the creation of TRACMIP and of CMIP6. The model data used in this study are available in Google cloud storage (https://console.cloud.google.com/storage/browser/cmip6) as a result of a grant to the Pangeo project (https://pangeo.io/).

REFERENCES

Andrews, T., J. M. Gregory, M. J. Webb, and K. E. Taylor, 2012: Forcing, feedbacks and climate sensitivity in CMIP5 coupled atmosphere–ocean climate models. *Geophys. Res. Lett.*, **39**, L09712, https://doi.org/10.1029/2012GL051607.

——, ——, and ——, 2015: The dependence of radiative forcing and feedback on evolving patterns of surface temperature change in climate models. *J. Climate*, **28**, 1630–1648, https://doi.org/10.1175/JCLI-D-14-00545.1.

Armour, K. C., C. M. Bitz, and G. H. Roe, 2013: Time-varying climate sensitivity from regional feedbacks. *J. Climate*, **26**, 4518–4534, https://doi.org/10.1175/JCLI-D-12-00544.1.

Atwood, A. R., A. Donohoe, D. S. Battisti, X. Liu, and F. S. R. Pausata, 2020: Robust longitudinally variable responses of the ITCZ to a myriad of climate forcings. *Geophys. Res. Lett.*, **47**, e2020GL088833, https://doi.org/10.1029/2020GL088833.

Back, L. E., and C. S. Bretherton, 2009: On the relationship between SST gradients, boundary layer winds, and convergence over the tropical oceans. *J. Climate*, **22**, 4182–4196, https://doi.org/10.1175/2009JCLI2392.1.

Bellomo, K., A. Clement, T. Mauritsen, G. Rädel, and B. Stevens, 2014: Simulating the role of subtropical stratocumulus clouds in driving Pacific climate variability. *J. Climate*, **27**, 5119–5131, https://doi.org/10.1175/JCLI-D-13-00548.1.

Biasutti, M., and Coauthors, 2018: Global energetics and local physics as drivers of past, present and future monsoons. *Nat. Geosci.*, **11**, 392–400, https://doi.org/10.1038/s41561-018-0137-1.

Bordoni, S., and T. Schneider, 2008: Monsoons as eddy-mediated regime transitions of the tropical overturning circulation. *Nat. Geosci.*, **1**, 515–519, https://doi.org/10.1038/ngeo248.

Chadwick, R., P. Good, T. Andrews, and G. Martin, 2014: Surface warming patterns drive tropical rainfall pattern responses to CO_2 forcing on all timescales. *Geophys. Res. Lett.*, **41**, 610–615, https://doi.org/10.1002/2013GL058504.

Chiang, J., and D. Vimont, 2004: Analogous Pacific and Atlantic meridional modes of tropical atmosphere–ocean variability. *J. Climate*, **17**, 4143–4158, https://doi.org/10.1175/JCLI4953.1.

——, M. Biasutti, and D. Battisti, 2003: Sensitivity of the Atlantic Intertropical Convergence Zone to Last Glacial Maximum boundary conditions. *Paleoceanogr. Paleoclimatol*, **18**, 1094, https://doi.org/10.1029/2003PA000916.

Chou, C., J. Neelin, and H. Su, 2001: Ocean–atmosphere–land feedbacks in an idealized monsoon. *Quart. J. Roy. Meteor. Soc.*, **127**, 1869–1891, https://doi.org/10.1002/qj.49712757602.

Clement, A., P. N. DiNezio, and C. Deser, 2011: Rethinking the ocean's role in the Southern Oscillation. *J. Climate*, **24**, 4056–4072, https://doi.org/10.1175/2011JCLI3973.1.

Donohoe, A., and D. S. Battisti, 2011: Atmospheric and surface contributions to planetary albedo. *J. Climate*, **24**, 4402–4418, https://doi.org/10.1175/2011JCLI3946.1.

Emanuel, K., J. Neelin, and C. S. Bretherton, 1994: On large-scale circulations in convecting atmospheres. *Quart. J. Roy. Meteor. Soc.*, **120**, 1111–1143, https://doi.org/10.1002/qj.49712051902.

Eyring, V., S. Bony, G. A. Meehl, C. A. Senior, B. Stevens, R. J. Stouffer, and K. E. Taylor, 2016: Overview of the Coupled Model Intercomparison Project Phase 6 (CMIP6) experimental design and organization. *Geosci. Model Dev.*, **9**, 1937–1958, https://doi.org/10.5194/gmd-9-1937-2016.

Feldl, N., S. Bordoni, and T. M. Merlis, 2017: Coupled high-latitude climate feedbacks and their impact on atmospheric heat transport. *J. Climate*, **30**, 189–201, https://doi.org/10.1175/JCLI-D-16-0324.1.

Gill, A. E., 1980: Some simple solutions for heat-induced tropical circulation. *Quart. J. Roy. Meteor. Soc.*, **106**, 447–462, https://doi.org/10.1002/qj.49710644905.

Gregory, J., and M. Webb, 2008: Tropospheric adjustment induces a cloud component in CO_2 forcing. *J. Climate*, **21**, 58–71, https://doi.org/10.1175/2007JCLI1834.1.

——, and Coauthors, 2004: A new method for diagnosing radiative forcing and climate sensitivity. *Geophys. Res. Lett.*, **31**, L03205, https://doi.org/10.1029/2003GL018747.

Huffman, G., R. F. Adler, E. Stocker, D. T. Bolvin, and E. Nelkin, 2003: Analysis of TRMM 3-hourly multi-satellite precipitation estimates computed in both real and post-real time. *Twelfth Conf. on Satellite Meteorology and Oceanography*, Long Beach, CA, Amer. Meteor. Soc., P4.11.

Lindzen, R., and S. Nigam, 1987: On the role of sea surface temperature gradients in forcing low-level winds and convergence in the tropics. *J. Atmos. Sci.*, **44**, 2418–2436, https://doi.org/10.1175/1520-0469(1987)044<2418:OTROSS>2.0.CO;2.

Lintner, B. R., and J. Neelin, 2007: A prototype for convective margin shifts. *Geophys. Res. Lett.*, **34**, L05812, https://doi.org/10.1029/2006GL027305.

Maroon, E. A., and D. M. W. Frierson, 2016: The impact of a continent's longitudinal extent on tropical precipitation. *Geophys. Res. Lett.*, **43**, 11 921–11 929, https://doi.org/10.1002/2016GL071518.

——, ——, and D. S. Battisti, 2014: The tropical precipitation response to Andes topography and ocean heat fluxes in an aquaplanet model. *J. Climate*, **28**, 381–398, https://doi.org/10.1175/JCLI-D-14-00188.1.

Marshall, J., A. Donohoe, D. Ferreira, and D. McGee, 2014: The ocean's role in setting the mean position of the Inter-Tropical Convergence Zone. *Climate Dyn.*, **42**, 1967–1979, https://doi.org/10.1007/s00382-013-1767-z.

Pendergrass, A. G., A. Conley, and F. M. Vitt, 2018: Surface and top-of-atmosphere radiative feedback kernels for CESM-CAM5. *Earth Syst. Sci. Data*, **10**, 317–324, https://doi.org/10.5194/essd-10-317-2018.

Philander, S. G. H., D. Gu, D. Halpern, G. Lambert, N. Lau, T. Li, and R. C. Pacanowski, 1996: Why the ITCZ is mostly north of the equator. *J. Climate*, **9**, 2958–2972, https://doi.org/10.1175/1520-0442(1996)009<2958:WTIIMN>2.0.CO;2.

Reynolds, R. W., and T. Smith, 1994: Improved global sea surface temperature analyses. *J. Climate*, **7**, 929–948, https://doi.org/10.1175/1520-0442(1994)007<0929:IGSSTA>2.0.CO;2.

Russotto, R. D., and M. Biasutti, 2020: Polar amplification as an inherent response of a circulating atmosphere: Results from the TRACMIP aquaplanets. *Geophys. Res. Lett.*, **47**, e2019GL086771, https://doi.org/10.1029/2019GL086771.

Seager, R., M. Cane, N. Henderson, D. E. Lee, R. Abernathey, and H. Zhang, 2019: Strengthening tropical Pacific zonal sea surface temperature gradient consistent with rising greenhouse gases. *Nat. Climate Change*, **9**, 517–522, https://doi.org/10.1038/s41558-019-0505-x.

Takahashi, K., and D. S. Battisti, 2007: Processes controlling the mean tropical Pacific precipitation pattern. Part I: The Andes and the eastern Pacific ITCZ. *J. Climate*, **20**, 3434–3451, https://doi.org/10.1175/JCLI4198.1.

Taylor, K. E., M. Crucifix, P. Braconnot, C. D. Hewitt, C. Doutriaux, A. J. Broccoli, J. F. B. Mitchell, and M. J. Webb, 2007: Estimating shortwave radiative forcing and response in climate models. *J. Climate*, **20**, 2530–2543, https://doi.org/10.1175/JCLI4143.1.

Voigt, A., and Coauthors, 2016: The Tropical Rain belts with an Annual cycle and a Continent Model Intercomparison Project: TRACMIP. *J. Adv. Model. Earth Syst.*, **8**, 1868–1891, https://doi.org/10.1002/2016MS000748.

Xie, S.-P., and S. G. H. Philander, 1994: A coupled ocean–atmosphere model of relevance to the ITCZ in the eastern Pacific. *Tellus*, **46**, 340–350, https://doi.org/10.3402/tellusa.v46i4.15484.

Zhou, W., and S.-P. Xie, 2017: Intermodel spread of the double-ITCZ bias in coupled GCMs tied to land surface temperature in AMIP GCMs. *Geophys. Res. Lett.*, **44**, 7975–7984, https://doi.org/10.1002/2017GL074377.

——, and ——, 2018: A hierarchy of idealized monsoons in an intermediate GCM. *J. Climate*, **31**, 9021–9036, https://doi.org/10.1175/JCLI-D-18-0084.1.